

Semantically Plausible and Diverse 3D Human Motion Prediction

Sadegh Aliakbarian^{1,2}, Fatemeh Saleh^{1,2}, Mathieu Salzmann³, Lars Petersson⁴, Stephen Gould^{1,2}

¹Australian National University, ²ACRV, ³CVLab, EPFL, ⁴Data61, CSIRO

Abstract

We tackle the task of diverse 3D human motion prediction, that is, forecasting multiple plausible future 3D poses given a sequence of observed 3D poses. In this context, a popular approach consists of using Conditional Variational Autoencoders (CVAEs). Existing approaches to generate diverse motions either fail to capture the diversity in human motion or fail to generate diverse but semantically plausible continuations of an observed motion. In this paper, we address both of these problems by developing a new variational framework that accounts for both diversity and semantic of the generated future motion. Unlike existing approaches that sampling the latent variable is independent of the conditioning, our approach conditions the sampling process of the latent variable on the representation of the past observation, thus encouraging it to carry relevant information. Our experiments demonstrate that our approach not only yields motions of higher quality while retaining diversity, but also generates motions that preserve semantic information contained in the observed 3D pose sequence.

1. Introduction

Human motion prediction is the task of forecasting plausible 3D human motion continuation(s) given a sequence of past 3D human poses. To address this problem, prior work mostly relies on recurrent encoder-decoder architectures, where the encoder processes the observed motion, and the decoder generates a single estimated future trajectory given the encoded representation of the past [21, 10, 26, 15, 4, 22, 23, 20]. While this approach yields valid future motion, it tends to ignore the fact that human motion is stochastic in nature; given one single observation, multiple diverse continuations of the motion are likely and plausible. The lack of stochasticity of these encoder-decoder methods ensues from the fact that both the network operations and the sequences in the training dataset are deterministic¹. In this paper, we introduce an approach to modeling

this stochasticity by learning *multiple modes* of human motion. We focus on generating both diverse and semantically plausible motion prediction. By semantically plausible, we mean motions that are natural continuations of an observed sequence of 3D poses that preserve and continue the context that happened in the observation. For instance, we *mostly* expect different plausible modes of “Walking” when the human is walking in the observation.

Recent attempts that account for human motion stochasticity rely on combining a random vector with an encoding of the observed pose sequence [6, 28, 4, 26, 15, 18, 3]. In particular, the state-of-the-art approaches to diverse human motion prediction [3, 28] make use of conditional variational autoencoders (CVAEs). In this paper, we argue that standard CVAEs are ill-suited to generate motions that are diverse *and* semantically plausible for the following reasons:

(1) Standard CVAE framework struggles at capturing the diversity in generated motions when the conditioning signal (i.e., the observed 3D motion) is strong. In the case of human motion prediction, in particular, the past observation *is* a strong representation such that an expressive motion decoder can generate a natural continuation given only the condition [3, 28]. In this case, the deterministic conditioning scheme, e.g., concatenation as in standard CVAEs, allows the model to learn to ignore the latent variable and only focus on the condition to minimize the reconstruction loss. Ignoring the latent variable also results in the KL divergence of (close to) zero, and thus, the model reaches to an undesirable equilibrium.

(2) Although there exist techniques to prevent CVAEs from ignoring the latent variable [3] by replacing the deterministic conditioning scheme with a stochastic alternative, CVAEs suffers from another weakness: During training, CVAEs rely on a global prior on the latent variable, thus making it independent of the conditioning signal. At inference, this translates to sampling latent variables that do not *necessarily* match the given CVAE condition. We elaborate this observation in Section 3 when we describe the motivation to design our approach.

¹For complicated tasks such as motion prediction, the training data is typically insufficiently sampled, in that, for any given condition, the dataset contains only a single sample, in effect making the data appear deterministic.

tic. For instance, in motion prediction, we never observed twice the same past motion with two different future ones.

In this paper, we directly address these weaknesses by conditioning the sampling of the latent variable on the past 3D observation, thus encouraging the latent variable to carry relevant information. This also allows us to not rely on deterministic conditioning, as we elaborate in our experiments. Our extensive experiments show that not only does our approach yield a much wider variety of plausible samples than state-of-the-art stochastic motion prediction methods, but it also preserves the semantic information of the condition, such as the type of action performed by the person, without explicitly exploiting this information.

2. Related Work

Most motion prediction methods are based on *deterministic* models [23, 20, 22, 10, 13, 21, 11, 8, 9], casting motion prediction as a regression task where only one outcome is possible given the observation. While this may produce accurate predictions, it fails to reflect the stochastic nature of human motion, where multiple futures can be highly likely for a single given series of observations. Modeling stochasticity is the topic of this paper, and we therefore focus the discussion below on the other methods that have attempted to do so.

The general trend to incorporate variations in the predicted motions consists of combining information about the observed pose sequence with a random vector. In this context, two types of approaches have been studied: The techniques that directly incorporate the random vector into the RNN decoder and those that make use of an additional CVAE. In the first class of methods, [18] samples a random vector $z_t \sim \mathcal{N}(0, I)$ at each time step and adds it to the pose input of the RNN decoder. By relying on different random vectors at each time step, however, this strategy is prone to generating discontinuous motions. To overcome this, [15] makes use of a single random vector to generate the entire sequence. As we will show in our experiments, by relying on concatenation, these two methods contain parameters that are specific to the random vector, and thus give the model the flexibility to ignore this information. In [4], instead of using concatenation, the random vector is added to the hidden state produced by the RNN encoder. While addition prevents having parameters that are specific to the random vector, this vector is first transformed by multiplication with a learnable parameter matrix, and thus can again be zeroed out so as to remove the source of diversity, as observed in our experiments.

The second category of stochastic methods introduce an additional CVAE between the RNN encoder and decoder. In this context, [26] proposes to directly use the pose as conditioning variable. As will be shown in our experiments, while this approach is able to maintain some degree of diversity, albeit less than ours, it yields motions of lower quality because of its use of independent random vectors at each

time step. Instead of perturbing the pose, [28] uses the RNN decoder hidden state as conditioning variable in the CVAE, concatenating it with the random vector. While this approach generates high-quality motions, it suffers from the fact that the CVAE decoder gives the model the flexibility to ignore the random vector, which therefore yields low-diversity outputs. To overcome this, [3] perturbs the hidden states via a stochastic Mix-and-Match operation instead of concatenation. Through such a perturbation, the decoder is not able to decouple the noise and the condition. However, since the perturbation is not learned and is a non-parametric operation, the quality and the context of the generated motion are inferior to those obtained with our approach. More importantly, all of the above-mentioned CVAE-based approaches use priors that are independent of the condition. We will show in our experiments that such designs are ill-suited for human motion prediction. By contrast, our approach uses a conditional prior and is thus able to generate diverse motions of higher quality, carrying the contextual information of the conditioning signal.

3. Motivation

In essence, VAEs utilize neural networks to learn the distribution of the data. To this end, VAEs first learn to generate a latent variable z given the data x , i.e., approximate the posterior distribution $q_\phi(z|x)$, where ϕ are the parameters of a neural network, the encoder, whose goal is to model the variation of the data. From this latent random variable z , VAEs then generate a new sample x by learning $p_\theta(x|z)$, where θ denotes the parameters of another neural network, the decoder, whose goal is to maximize the log likelihood of the data. These two networks, i.e., the encoder and the decoder, are trained jointly, using a prior over the latent variable. By using a variational approximation of the posterior, training translates to maximizing the variational lower bound of the log likelihood with respect to the parameters ϕ and θ , given by

$$\log p_\theta(x) \geq \mathbb{E}_{q_\phi(z|x)} \left[\log p_\theta(x|z) \right] - KL(q_\phi(z|x) || p(z)), \quad (1)$$

where the second term on the right hand side encodes the KL divergence between the posterior $q_\phi(z|x)$ and a chosen prior distribution $p(z)$. As an extension to VAEs, CVAEs use auxiliary information, i.e., the conditioning variable or observation, to generate the data x . In the standard setting, both the encoder and the decoder are conditioned on the conditioning variable c . That is, the encoder becomes $q_\phi(z|x, c)$ and the decoder $p_\theta(x|z, c)$. Then, in theory, the

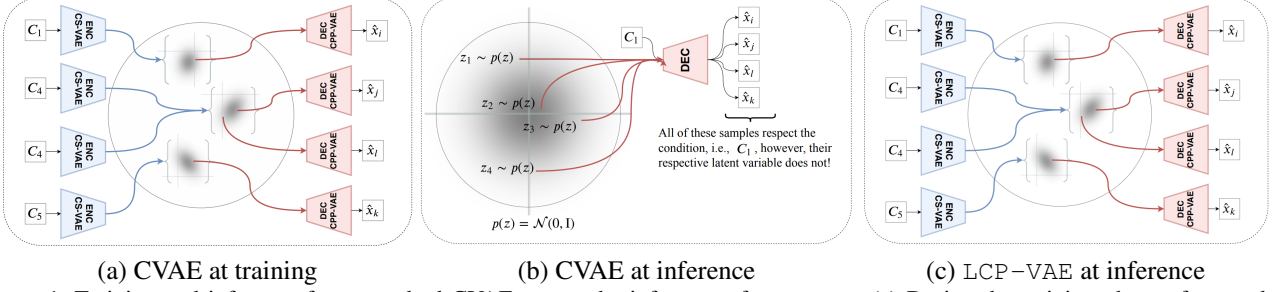


Figure 1. Training and inference for a standard CVAE versus the inference of LCP-VAE. (a) During the training phase of a standard CVAE, the encoder takes as input the combination of the data and the corresponding condition and compresses it into the latent space. The decoder then samples a latent variable from the approximate posterior computed by the encoder, combines the latent variable with the conditioning signal, and reconstructs the data. The approximate posterior distribution of all training samples, i.e., for all conditioning signals, is encouraged to match the prior distribution. (b) During inference of a standard CVAE, the decoder samples different latent variables from the prior distribution, combines them with the condition, and generates samples that all respect the conditioning signal. However, there is no guarantee that the latent variable is sampled from the region of the prior that corresponds to the given condition. (c) In LCP-VAE, at inference time, since we have access to the conditioning signal, we use the CS-VAE encoder to approximate the posterior of each condition. To generate a sample given a condition, the LCP-VAE decoder then samples a latent variable from the posterior of its condition, instead of using a general prior distribution as in CVAEs, and generate a sample. For instance, \hat{x}_j and \hat{x}_l are conditioned on C_4 and their corresponding latent variables are sampled from a very similar region. By contrast, \hat{x}_k is generated by a latent variable sampled from a completely different region, i.e., the region corresponding to the approximate posterior of C_5 .

objective of the model should become

$$\log p_\theta(x|c) \geq \mathbb{E}_{q_\phi(z|x,c)} \left[\log p_\theta(x|z,c) \right] - KL(q_\phi(z|x,c) || p(z|c)). \quad (2)$$

In practice, however, *the prior distribution of the latent variable is still assumed to be independent of c , i.e., $p(z | c) = p(z)$* . As illustrated by Fig. 1, at test time, this translates to sampling a latent variable from a region of the prior that is unlikely to be highly correlated with the (observed) condition.

In this paper, we overcome this limitation by explicitly making the sampling of the latent variable depend on the condition. In other words, instead of using $p(z)$ as prior distribution, we truly use $p(z|c)$. This not only respects the theory behind the design of CVAEs, but, as we empirically demonstrate, leads to generating motions of higher quality, that preserve the context of the conditioning signal, i.e., the observed past motion. To achieve this, we develop a CVAE architecture that learns a distribution not only of the latent variable but also of the conditioning one. We then use this distribution as a prior over the latent variable, making its sampling explicitly dependent on the condition.

4. Our Approach

In this section, we describe our approach, LCP-VAE, for VAEs with Learned Conditional Priors, for generating diverse and plausible continuations of 3D human pose sequences, where the latent variables are sampled from an appropriate region of the prior distribution. In essence,

our framework consists of two autoencoders, one acting on the past observed sequence of 3D poses (i.e., the conditioning signal) and the other on the future sequence of 3D poses (i.e., the continuation of the motion) which we wish to model. The latent representation of the condition then serves as a conditioning variable to generate motions from a learned distribution.

As discussed in Section 3, our approach forces the sampling of the random latent variable to depend on the conditioning one. By making this dependency explicit, we (1) sample an informative latent variable *given* the condition, and thus generate motions of higher quality that preserve the context of the observed motion, and (2) prevent the network from ignoring the latent variable in the presence of a strong condition, thus enabling it to generate diverse outputs.

Note that conditioning the VAE *encoder* via standard strategies, e.g., concatenation, is perfectly fine, since the two inputs to the encoder, i.e., the data and the condition, are deterministic and useful to compress the sample into the latent space. However, conditioning the VAE *decoder* requires special care, which is what we focus on below.

4.1. Stochastically Conditioning the Decoder

We propose to make the sampling of the latent variable from the prior/posterior distribution explicitly depend on the condition instead of treating these two variables as independent. To this end, we first learn the distribution of the condition via a simple VAE, which we refer to as CS-VAE because this VAE acts on the conditioning signal. The goal of CS-VAE is to reconstruct the condition,

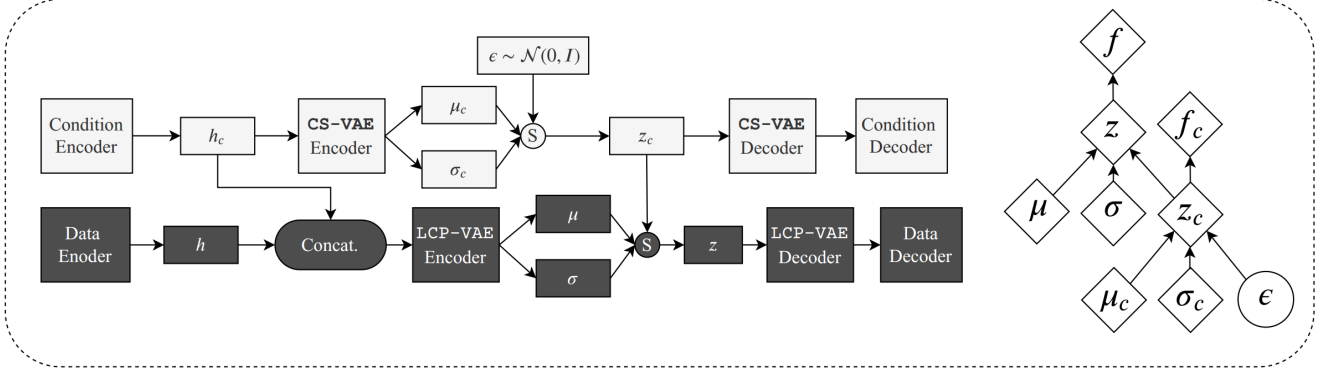


Figure 2. In an LCP-VAE, the sampling of z is conditioned on the CVAE condition via the latent variable z_c . Specifically, the posterior distribution of the condition acts as prior on the data posterior. This corresponds to the *extended reparameterization trick* illustrated on the right. Note that the approximate posterior is not normally distributed anymore.

e.g., the observed past motion, given its latent representation. We take the prior of CS-VAE as a standard Normal distribution $\mathcal{N}(0, I)$. Following Kingma and Welling [14], this allows us to approximate the CS-VAE posterior with another sample from a Normal distribution $\epsilon \sim \mathcal{N}(0, I)$ via the reparameterization trick

$$z_c = \mu_c + \sigma_c \odot \epsilon, \quad (3)$$

where μ_c and σ_c are the parameter vectors of the posterior distribution generated by the VAE encoder, and thus $z_c \sim \mathcal{N}(\mu_c, \text{diag}(\sigma_c)^2)$.

Following the same strategy for the data VAE translates to treating the conditioning and the data latent variables independently, which we seek to avoid. Therefore, as illustrated in Fig. 2 (Bottom), we instead define the LCP-VAE posterior not as directly normally distributed but conditioned on the posterior of CS-VAE. To this end, we extend the standard reparameterization trick as

$$\begin{aligned} z &= \mu + \sigma \odot z_c \\ &= \mu + \sigma \odot (\mu_c + \sigma_c \odot \epsilon) \\ &= \underbrace{(\mu + \sigma \odot \mu_c)}_{\text{LCP-VAE's mean}} + \underbrace{(\sigma \odot \sigma_c)}_{\text{LCP-VAE's std.}} \odot \epsilon, \end{aligned} \quad (4)$$

where z_c comes from Eq. 3, and μ and σ are the parameter vectors generated by the LCP-VAE encoder. In fact, z_c in Eq. 3 is a sample from the scaled and translated version of $\mathcal{N}(0, I)$ given μ_c and σ_c , and z in Eq. 4 is a sample from the scaled and translated version of $\mathcal{N}(\mu_c, \text{diag}(\sigma_c)^2)$ given μ and σ . Since we have access to the observations during both training and testing, we always sample z_c from the condition posterior. As z is sampled given z_c , one expects the latent variable z to carry information about the strong condition, and thus a sample generated from z to correspond to a plausible sample given the condition. This extended reparameterization trick lets us sample one single informative latent variable that contains information about both the

data and the conditioning signal. This further allows us to avoid conditioning the LCP-VAE decoder by concatenating the latent variable with a deterministic representation of the condition.

Note that our sampling strategy changes the variational family of the LCP-VAE posterior. In fact, the posterior is no longer $\mathcal{N}(\mu, \text{diag}(\sigma)^2)$, but a Gaussian distribution with mean $\mu + \sigma \odot \mu_c$ and covariance matrix $\text{diag}(\sigma \odot \sigma_c)^2$. This will be accounted for when designing the KL divergence loss discussed below.

4.2. Learning

To learn the parameters of our model, we rely on the availability of a dataset $D = \{X_1, X_2, \dots, X_N\}$ containing N training motion sequences X_i s. Each motion consists of a sequence of T poses, $X_i = \{x_i^1, x_i^2, \dots, x_i^T\}$, and each pose comprises J joints forming a skeleton, $x_i^t = \{x_{i,1}^t, x_{i,2}^t, \dots, x_{i,J}^t\}$. The pose of each joint is represented as a 4D quaternion. Each training sample X_i is a pair of past observed motion or condition, $x_i^{1:t}$, and future motion, $x_i^{t+1:T}$. For CS-VAE, which learns the distribution of the condition, we define the loss as the KL divergence between its posterior and the standard Gaussian prior, that is,

$$\begin{aligned} \mathcal{L}_{\text{prior}}^{\text{CS-VAE}} &= KL\left(\mathcal{N}(\mu_c, \text{diag}(\sigma_c)^2) \parallel \mathcal{N}(0, I)\right) \\ &= -\frac{1}{2} \sum_{j=1}^d \left(1 + \log(\sigma_{c_j}^2) - \mu_{c_j}^2 - \sigma_{c_j}^2\right), \end{aligned} \quad (5)$$

where d is the dimension of the latent variable z_c . By contrast, for LCP-VAE, we define the loss as the KL divergence between the posterior of LCP-VAE and the posterior of CS-VAE, i.e., of the condition. To this end, we freeze the weights of CS-VAE before computing the KL divergence, since we do not want to move the posterior of the condition but that of the data. The KL divergence is then computed as the divergence between two multivariate Normal distri-

butions, encoded by their mean vectors and covariance matrices as

$$\mathcal{L}_{prior}^{LCP-VAE} = KL\left(\mathcal{N}(\mu + \sigma \odot \mu_c, \text{diag}(\sigma \odot \sigma_c)^2) \parallel \mathcal{N}(\mu_c, \text{diag}(\sigma_c)^2)\right). \quad (6)$$

Let $\Sigma = \text{diag}(\sigma)^2$, $\Sigma_c = \text{diag}(\sigma_c)^2$, d be the dimensionality of the latent space and $\text{tr}\{\cdot\}$ the trace of a square matrix. The loss in Eq. 6 can be written as²

$$\begin{aligned} \mathcal{L}_{prior}^{LCP-VAE} = & -\frac{1}{2} \left[\log \frac{1}{|\Sigma|} - d + \text{tr}\{\Sigma\} \right. \\ & \left. + (\mu_c - (\mu + \Sigma\mu_c))^T \Sigma_c^{-1} (\mu_c - (\mu + \Sigma\mu_c)) \right]. \end{aligned} \quad (7)$$

After computing the loss in Eq. 7, we unfreeze CS-VAE and update it with its previous gradient. Trying to match the posterior of LCP-VAE to that of CS-VAE allows us to effectively use our extended reparameterization trick in Eq. 4. Furthermore, we use the standard reconstruction loss for both CS-VAE and LCP-VAE, thus minimizing the mean squared error (MSE) as

$$\mathcal{L}_{rec}^{CS-VAE} = - \sum_{k=1}^t \sum_{j=1}^J \|\hat{x}_{i,j}^k - x_{i,j}^k\|^2, \quad (8)$$

for CS-VAE, and

$$\mathcal{L}_{rec}^{LCP-VAE} = - \sum_{k=t+1}^T \sum_{j=1}^J \|\hat{x}_{i,j}^k - x_{i,j}^k\|^2, \quad (9)$$

for LCP-VAE. Thus, our complete loss is

$$\mathcal{L} = \lambda(\mathcal{L}_{prior}^{CS-VAE} + \mathcal{L}_{prior}^{LCP-VAE}) + \mathcal{L}_{rec}^{CS-VAE} + \mathcal{L}_{rec}^{LCP-VAE}. \quad (10)$$

In practice, since the nature of our data is sequential (e.g., sequence of human poses in human motion prediction and sequence of words in image captioning), the LCP-VAE encoder is a recurrent model. Thus, we weigh the KL divergence terms by a function λ corresponding to the KL annealing weight of [5], which follows the standard practice in diverse human motion prediction [28, 26, 3]. We start from $\lambda = 0$, forcing the model to encode as much information in z as possible, and gradually increase it to $\lambda = 1$ during training, following a logistic curve. We then continue training with $\lambda = 1$.

In short, our method can be interpreted as a simple yet effective framework (designed for CVAEs) for altering the

²See the supplementary material for more detail on the KL divergence between two multivariate Gaussians and the derivation of Eq. 7.

Table 1. Comparison of LCP-VAE with the stochastic motion prediction baselines on Human3.6M (top) and CMU MoCap (bottom).

Results on Human3.6M				
Method	Test MSE (KL) (Reconstructed)	Diversity (Sampled)	Quality (Sampled)	Context (Sampled)
MT-VAE [28]	0.51 (0.06)	0.26	0.45	0.42
Pose-Knows [26]	2.08 (N/A)	1.70	0.13	0.08
HP-GAN [4]	0.61 (N/A)	0.48	0.47	0.35
Mix-and-Match [3]	0.55 (2.03)	3.52	0.42	0.37
LCP-VAE	0.41 (8.07)	3.12	0.48	0.54

Results on CMU MoCap				
Method	ELBO (KL) (Reconstructed)	Diversity (Sampled)	Quality (Sampled)	Context (Sampled)
MT-VAE [28]	0.25 (0.08)	0.41	0.46	0.80
Pose-Knows [26]	1.93 (N/A)	3.00	0.18	0.27
HP-GAN [4]	0.24 (N/A)	0.43	0.45	0.73
Mix-and-Match [3]	0.25 (2.92)	2.63	0.46	0.78
LCP-VAE	0.23 (4.13)	2.36	0.48	0.88

Table 2. Comparison of the generated motions with the ground-truth future motions in terms of context. The gap between the performance of the state-of-the-art pose-based action classifier [17] with and without true future motions is 0.22 / 0.54. Using our predictions, this gap decreases to 0.06 / 0.08, showing that our predictions reflect the class label. H3.6M / CMU represent Human3.6M and CMU MoCap, respectively.

Setting	Obs.	Future Motion	Context (H3.6M / CMU)
Lower bound	GT	Zero velocity	0.38 / 0.42
Upper bound	GT	GT	0.60 / 0.96
Ours	GT	Sampled from LCP-VAE	0.54 / 0.88

variational family of the posterior such that (1) a latent variable from this posterior distribution is explicitly sampled given the condition, both during training and inference (as illustrated in Fig. 1), and (2) the model is much less likely to suffer from posterior collapse because the mismatch between the posterior and prior distributions makes it harder for learning to drive the KL divergence of Eq. 7 towards zero.

5. Experiments

To evaluate the effectiveness of our approach on the task of stochastic human motion prediction, we use the Human3.6M [12] and CMU MoCap³ datasets, two large publicly-available motion capture (mocap) datasets. While we use both datasets for comparisons to the state of the art, for all ablation studies, we only report on Human3.6M dataset.

Datasets. Human3.6M comprises more than 800 long indoor motion sequences performed by 11 subjects, leading to 3.6M frames. Each frame contains a person annotated with 3D joint positions and rotation matrices for all 32 joints. In

³Available at <http://mocap.cs.cmu.edu/>.



Figure 3. Qualitative evaluation of the diversity in human motion. The first row depicts the ground-truth motion. The first six poses of each row correspond to the observation (the condition) and the rest are sampled from our model. Each row is a randomly sampled motion (not cherry picked). Note that all sampled motions are natural, with a smooth transition from the observed poses to the generated ones. Diversity increases with the length of the generated sequence.

our experiments, for our approach and the replicated VAE-based baselines, we represent each joint in 4D quaternion space. We follow the standard preprocessing and evaluation settings used in [21, 10, 23, 13, 3]. The CMU MoCap dataset is another large-scale motion capture dataset covering diverse human activities, such as jumping, running, walking, and playing basketball. Each frame contains a person annotated with 3D joint rotation matrices for all 38 joints. As for Human3.6M, and following standard practice [20, 16], we represent each joint in 4D quaternion space. We also evaluate our approach on the real-world Penn Action dataset [31], which contains 2326 sequences of 15 different actions, where for each person, 13 joints are annotated in 2D space. The results on Penn Action are provided in the supplementary material.

Evaluation Metrics. To quantitatively evaluate our approach and other stochastic motion prediction baselines [28, 4, 26, 3], we report the test reconstruction error, along with the KL-divergence on the held-out test set. Additionally, we report quality [3] and diversity [29, 3, 30] metrics, which should be considered together. Specifically, to measure the diversity of the motions generated by a stochastic model, we make use of the average distance between all pairs of the K motions generated from the same observation. To mea-

sure quality, following the quality metric of [3], we train a binary classifier [3] to discriminate real (ground-truth) samples from fake (generated) ones. The accuracy of this classifier on the test set is inversely proportional to the quality of the generated motions. Note that, through extensive evaluations, Aliakbarian et al., [3] demonstrate that the results of human evaluation match those of the classifier-based quality metric. Furthermore, we report a context metric measured as the performance of a strong action classifier [17] trained on ground-truth motions. Specifically, the classifier is tested on each of the K motions generated from each observation. For N observations and K continuations per observation, the accuracy is measured by computing the argmax over each prediction’s probability vector, and we report context as the mean class accuracy on the $K \times N$ motions. Unless otherwise stated, for all metrics, we use $K = 50$ motions per test observation. Similarly, for all experiments, we use 16 frames (i.e., 640ms) as observation to generate the next 60 frames (i.e., 2.4sec).

Comparison to the State of the Art. In Table 1, we compare our approach (whose detailed architecture is described in the supplementary material) with the state-of-the-art stochastic motion prediction models [28, 3, 26, 4]. Note that, when evaluating stochastic motion prediction

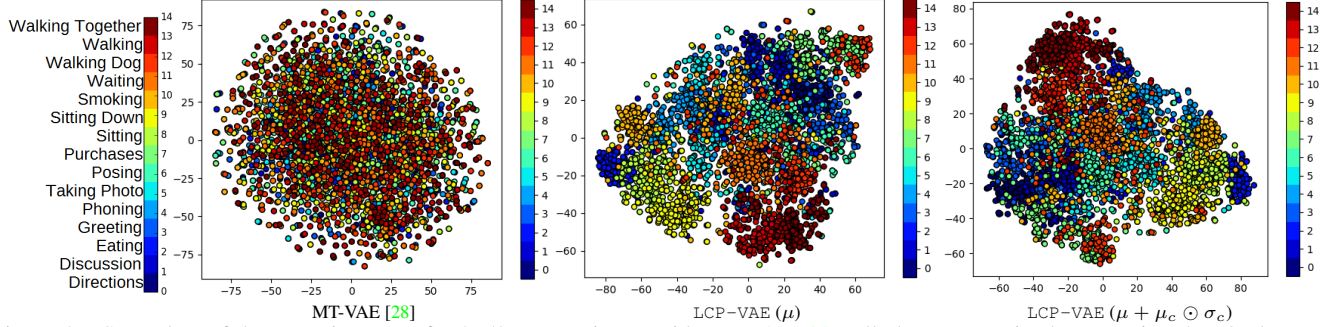


Figure 4. t-SNE plots of the posterior mean for 3750 test motions. With MT-VAE [28], all classes are mixed, suggesting that the latent variable carries little information about the motions. By contrast, our condition-dependent sampling allows LCP-VAE to better preserve context. Note that some actions, such as discussion and directions, are very hard to identify and are thus spread over other actions. Others, such as walking, walking with dog, and walking together, or sitting and sitting down overlap due to their similarity.

Table 3. Comparison with the state-of-the-art stochastic motion prediction models for 4 actions of Human3.6M (all methods use the best of $K = 50$ sampled motions).

Method	Walking						Eating					
	80	160	320	400	560	1000	80	160	320	400	560	1000
MT-VAE [28]	0.73	0.79	0.90	0.93	0.95	1.05	0.68	0.74	0.95	1.00	1.03	1.38
HP-GAN [4]	0.61	0.62	0.71	0.79	0.83	1.07	0.53	0.67	0.79	0.88	0.97	1.12
Pose-Knows [26]	0.56	0.66	0.98	1.05	1.28	1.60	0.44	0.60	0.71	0.84	1.05	1.54
Mix&Match [3]	0.33	0.48	0.56	0.58	0.64	0.68	0.23	0.34	0.41	0.50	0.61	0.91
LCP-VAE	0.22	0.36	0.47	0.52	0.58	0.69	0.19	0.28	0.40	0.51	0.58	0.90

Method	Smoking						Discussion					
	80	160	320	400	560	1000	80	160	320	400	560	1000
MT-VAE [28]	1.00	1.14	1.43	1.44	1.68	1.99	0.80	1.01	1.22	1.35	1.56	1.69
HP-GAN [4]	0.64	0.78	1.05	1.12	1.64	1.84	0.79	1.00	1.12	1.29	1.43	1.71
Pose-Knows [26]	0.59	0.83	1.25	1.36	1.67	2.03	0.73	1.10	1.33	1.34	1.45	1.85
Mix&Match [3]	0.23	0.42	0.79	0.77	0.82	1.25	0.25	0.60	0.83	0.89	1.12	1.30
LCP-VAE	0.23	0.43	0.77	0.75	0.78	1.23	0.21	0.52	0.81	0.84	1.04	1.28

models, one should consider the reported metrics jointly to truly evaluate the performance of a stochastic model. For instance, while MT-VAE [28] and HP-GAN [4] generate high-quality motions, they are not diverse. Conversely, while Pose-Knows [26] generates diverse motions, they are of low quality. By contrast, our approach generates both high quality and diverse motions. This is also the case of Mix-and-Match [3], which, however, preserves much less contextual information and semantics of the observed motions. In fact, none of the baselines effectively conveys the semantic information of the observation to the generated motions. As shown in Table 2, the upper bound for context on Human3.6M is 0.60 (i.e., the classifier [17] performance given the ground-truth motions). Our approach yields a context of 0.54 when given only about 20% of the data. We observe a similar behavior on the CMU MoCap dataset, shown in Table 2. Altogether, as also supported by the qualitative results of Fig. 3 and in the supplementary material, our approach yields diverse, high-quality and context-preserving predictions. This is further evidenced by the t-SNE [19] plots of Fig. 4, where different samples of various actions are better separated for our approach than

Table 4. Comparison with the state-of-the-art deterministic models for 4 actions of Human3.6M. Note that in our approach, we use $z = \mu_c$ to generate a single motion.

Method	Walking						Eating					
	80	160	320	400	560	1000	80	160	320	400	560	1000
Zero Velocity	0.39	0.86	0.99	1.15	1.35	1.32	0.27	0.48	0.73	0.86	1.04	1.38
LSTM-3LR [8]	1.18	1.50	1.67	1.76	1.81	2.20	1.36	1.79	2.29	2.42	2.49	2.82
SRNN [13]	1.08	1.34	1.60	1.80	1.90	2.13	1.35	1.71	2.12	2.21	2.28	2.58
DAE-LSTM [9]	1.00	1.11	1.39	1.48	1.55	1.39	1.31	1.49	1.86	1.89	1.76	2.01
GRU [21]	0.28	0.49	0.72	0.81	0.93	1.03	0.23	0.39	0.62	0.76	0.95	1.08
AGED [10]	0.22	0.36	0.55	0.67	0.78	0.91	0.17	0.28	0.51	0.64	0.86	0.93
DCT-GCN [20]	0.18	0.31	0.49	0.56	0.65	0.67	0.16	0.29	0.50	0.62	0.76	1.12
LCP-VAE	0.20	0.34	0.48	0.53	0.57	0.71	0.20	0.26	0.44	0.52	0.61	0.92

Method	Smoking						Discussion					
	80	160	320	400	560	1000	80	160	320	400	560	1000
Zero Velocity	0.26	0.48	0.97	0.95	1.02	1.69	0.31	0.67	0.94	1.04	1.41	1.96
LSTM-3LR [8]	2.05	2.34	3.10	3.18	3.24	3.42	2.25	2.33	2.45	2.46	2.48	2.93
SRNN [13]	1.90	2.30	2.90	3.10	3.21	3.23	1.67	2.03	2.20	2.31	2.39	2.43
DAE-LSTM [9]	0.92	1.03	1.15	1.25	1.38	1.77	1.11	1.20	1.38	1.42	1.53	1.73
GRU [21]	0.33	0.61	1.05	1.15	1.25	1.50	0.31	0.68	1.01	1.09	1.43	1.69
AGED [10]	0.27	0.43	0.82	0.84	1.06	1.21	0.27	0.56	0.76	0.83	1.25	1.30
DCT-GCN [20]	0.22	0.41	0.86	0.80	0.87	1.57	0.20	0.51	0.77	0.85	1.33	1.70
LCP-VAE	0.21	0.43	0.79	0.79	0.77	1.15	0.22	0.55	0.79	0.81	1.05	1.28

for, e.g., MT-VAE [28].

Why existing methods fail to generate diverse, and plausible motions? In this section, we further analyse the behaviour of different baselines, as well as our approach under different evaluation metrics. We observed that MT-VAE model [28] tends to ignore the random variable z , thus ignoring the root of variation. As a consequence, it achieves a low diversity, much lower than ours, but produces samples of high quality, albeit almost identical. We empirically observed that the magnitude of the weights acting on z to be orders of magnitude smaller than that of acting on the condition, suggesting that MT-VAE [28] indeed has learned to ignore the latent variable. Similarly, our experiment shows that HP-GAN model [4] also achieves limited diversity of the generated motions despite its use of random noise during inference. Note that the authors of [4] mentioned in their paper that the random noise was added to the hid-

den state. This is due to the fact⁴ that in [4], z is linearly transformed by a learnable weight matrix W before being added to the motion representation. By analysing W , we observed that the magnitude of its parameters is almost zero, allowing HP-GAN [4] to ignore z . Unlike [28, 4], Pose-Knows [26] produces more diverse motions, however, the quality is very low. By inspecting their code⁵, we observed that the random vectors that are concatenated to the poses at each time-step are sampled independently of each other, which translates to discontinuities in the generated motions. The Mix-and-Match approach [3] yields generated motions with higher diversity and reasonable quality. The architecture of Mix-and-Match is very close to that of MT-VAE [28], but replaces the deterministic concatenation operation with a stochastic perturbation of the hidden state with the noise. Through such a perturbation, the decoder is not able to decouple the noise and the condition, by contrast with concatenation. However, since the perturbation is not learned and is not parametric, the quality of the generated motion is lower than ours and of other baselines (except for Pose-Knows [26]). We see the Mix-and-Match perturbation as a workaround to the deficiency of concatenation, which nonetheless sacrifices the quality and the semantic information of the sampled motions.

Evaluating Sampling Quality. To further evaluate the sampling quality, we evaluate stochastic baselines using the standard mean angle error (MAE) metric in Euler space. To this end, we use the best of the $K = 50$ generated motions for each observation (referred to as S-MSE in [28]). A model that generates more diverse motions has higher chances of producing a motion close to the ground-truth one. As shown in Table 3, this is the case with our approach and Mix-and-Match [3], which both yield higher diversity. However, our approach performs better thanks to its context-preserving latent representation and its higher quality of the generated motions. In Table 4, we compare our approach with the state-of-the-art deterministic motion prediction models [21, 13, 11, 8, 10] using the MAE metric in Euler space. To have a fair comparison, we generate one motion per observation by setting the latent variable to the distribution mode, i.e., $z = \mu_c$. This allows us to generate a plausible motion without having access to the ground truth. To compare against the deterministic baselines, we follow the standard setting, and thus use 50 frames (i.e., 2sec) as observation to generate the next 25 frames (i.e., 1sec). Surprisingly, despite having a very simple motion decoder architecture (one-layer GRU network) with a very simple reconstruction loss function (MSE), this motion-from-mode strategy yields results that are competitive with those of the baselines that use sophisticated architectures and advanced

Table 5. Evaluation of various architecture designs for a CVAE.

Encoder Conditioning	Decoder Conditioning	Diversity	Context
Concatenation (z_c)	Reparameterization (z_c)	3.35	0.51
Concatenation (h_t)	Concatenation (h_t)	0.24	0.43
Concatenation (z_c)	Concatenation (z_c)	1.28	0.40
Concatenation (h_t)	Reparameterization (z_c)	3.12	0.54

loss functions. We argue that learning a good, context-preserving latent representation of human motion is the contributing factor to the success of our approach. This, however, could be used in conjunction with sophisticated motion decoders and reconstruction losses, which we leave for future research.

Ablation Study on Different Means of Conditioning. We also study various designs to condition the VAE encoder and decoder. As discussed before, conditioning the VAE encoder can be safely done via concatenating two deterministic sources of information, i.e., the representations of the past and the future, since both sources are useful to compress the future motion into the latent space. In Table 5, we use both a deterministic representation of the observation, h_t , and a stochastic one, z_c , as a conditioning variable for the encoder. Similarly, we compare the use of either of these variables via concatenation with that of our extended reparameterization trick (Eq. 4). This shows that, to condition the decoder, reparameterization is highly effective at generating diverse and plausible motions. Furthermore, for the encoder, a deterministic condition works better than a stochastic one.

6. Conclusion

In this paper, we have studied the problem of conditionally generating diverse and contextually and semantically plausible 3D human motions. We show that existing CVAE-based approach fail to capture and generate diverse and/or plausible human motions. We have addressed these problems by forcing the sampling of the latent variable to depend on the past observed motions, which contrasts with standard CVAEs. By making this dependency explicit, the model receives a latent variable that carries information about the (context) of the past observed motions during both training and test time. This further prevents the network from ignoring the latent variable in the presence of a strong condition, thus enabling it to generate diverse outputs. We demonstrate that our approach can generate high quality diverse motions that carry out the semantics in the observed motion, such as the type of action performed by the person, without explicitly exploiting this information. This will have great impact on practical applications such as action anticipation [25, 24, 1], pedestrian intention forecasting [2], and computer-generated imagery (CGI) and animation.

⁴By studying and running their publicly available code on <https://github.com/ebarsoum/hpgan>.

⁵<https://github.com/puffin444/poseknows>

References

- [1] M. S. Aliakbarian, F. Saleh, B. Fernando, M. Salzmann, L. Petersson, and L. Andersson. Deep action-and context-aware sequence learning for activity recognition and anticipation. *arXiv preprint arXiv:1611.05520*, 2016. 8
- [2] M. S. Aliakbarian, F. S. Saleh, M. Salzmann, B. Fernando, L. Petersson, and L. Andersson. Viena2: A driving anticipation dataset. *arXiv preprint arXiv:1810.09044*, 2018. 8
- [3] S. Aliakbarian, F. S. Saleh, M. Salzmann, L. Petersson, and S. Gould. A stochastic conditioning scheme for diverse human motion prediction. In *The IEEE/CVF Conference on Computer Vision and Pattern Recognition (CVPR)*, June 2020. 1, 2, 5, 6, 7, 8
- [4] E. Barsoum, J. Kender, and Z. Liu. Hp-gan: Probabilistic 3d human motion prediction via gan. In *Proceedings of the IEEE Conference on Computer Vision and Pattern Recognition Workshops*, pages 1418–1427, 2018. 1, 2, 5, 6, 7, 8
- [5] S. R. Bowman, L. Vilnis, O. Vinyals, A. M. Dai, R. Jozefowicz, and S. Bengio. Generating sentences from a continuous space. *arXiv preprint arXiv:1511.06349*, 2015. 5
- [6] J. B  tepage, H. Kjellstr  m, and D. Kragic. Anticipating many futures: Online human motion prediction and generation for human-robot interaction. In *2018 IEEE International Conference on Robotics and Automation (ICRA)*, pages 1–9. IEEE, 2018. 1
- [7] J. Chung, C. Gulcehre, K. Cho, and Y. Bengio. Empirical evaluation of gated recurrent neural networks on sequence modeling. *arXiv preprint arXiv:1412.3555*, 2014. 10
- [8] K. Fragkiadaki, S. Levine, P. Felsen, and J. Malik. Recurrent network models for human dynamics. In *Proceedings of the IEEE International Conference on Computer Vision*, pages 4346–4354, 2015. 2, 7, 8
- [9] P. Ghosh, J. Song, E. Aksan, and O. Hilliges. Learning human motion models for long-term predictions. In *2017 International Conference on 3D Vision (3DV)*, pages 458–466. IEEE, 2017. 2, 7
- [10] L.-Y. Gui, Y.-X. Wang, X. Liang, and J. M. Moura. Adversarial geometry-aware human motion prediction. In *Proceedings of the European Conference on Computer Vision (ECCV)*, pages 786–803, 2018. 1, 2, 6, 7, 8
- [11] L.-Y. Gui, Y.-X. Wang, D. Ramanan, and J. M. Moura. Few-shot human motion prediction via meta-learning. In *Proceedings of the European Conference on Computer Vision (ECCV)*, pages 432–450, 2018. 2, 8
- [12] C. Ionescu, D. Papava, V. Olaru, and C. Sminchisescu. Human3.6m: Large scale datasets and predictive methods for 3d human sensing in natural environments. *IEEE Transactions on Pattern Analysis and Machine Intelligence*, 36(7):1325–1339, jul 2014. 5
- [13] A. Jain, A. R. Zamir, S. Savarese, and A. Saxena. Structural-rnn: Deep learning on spatio-temporal graphs. In *Proceedings of the IEEE Conference on Computer Vision and Pattern Recognition*, pages 5308–5317, 2016. 2, 6, 7, 8
- [14] D. P. Kingma and M. Welling. Auto-encoding variational bayes. *arXiv preprint arXiv:1312.6114*, 2013. 4, 12
- [15] J. N. Kundu, M. Gor, and R. V. Babu. Bihmp-gan: Bidirectional 3d human motion prediction gan. *arXiv preprint arXiv:1812.02591*, 2018. 1, 2
- [16] C. Li, Z. Zhang, W. Sun Lee, and G. Hee Lee. Convolutional sequence to sequence model for human dynamics. In *Proceedings of the IEEE Conference on Computer Vision and Pattern Recognition*, pages 5226–5234, 2018. 6
- [17] C. Li, Q. Zhong, D. Xie, and S. Pu. Co-occurrence feature learning from skeleton data for action recognition and detection with hierarchical aggregation. *arXiv preprint arXiv:1804.06055*, 2018. 5, 6, 7
- [18] X. Lin and M. R. Amer. Human motion modeling using dv-gans. *arXiv preprint arXiv:1804.10652*, 2018. 1, 2
- [19] L. v. d. Maaten and G. Hinton. Visualizing data using t-sne. *Journal of machine learning research*, 9(Nov):2579–2605, 2008. 7
- [20] W. Mao, M. Liu, M. Salzmann, and H. Li. Learning trajectory dependencies for human motion prediction. In *ICCV*, 2019. 1, 2, 6, 7
- [21] J. Martinez, M. J. Black, and J. Romero. On human motion prediction using recurrent neural networks. In *2017 IEEE Conference on Computer Vision and Pattern Recognition (CVPR)*, pages 4674–4683. IEEE, 2017. 1, 2, 6, 7, 8
- [22] D. Pavllo, C. Feichtenhofer, M. Auli, and D. Grangier. Modeling human motion with quaternion-based neural networks. *arXiv preprint arXiv:1901.07677*, 2019. 1, 2
- [23] D. Pavllo, D. Grangier, and M. Auli. Quaternet: A quaternion-based recurrent model for human motion. *arXiv preprint arXiv:1805.06485*, 2018. 1, 2, 6
- [24] C. Rodriguez, B. Fernando, and H. Li. Action anticipation by predicting future dynamic images. In *Proceedings of the European Conference on Computer Vision (ECCV)*, pages 0–0, 2018. 8
- [25] M. Sadegh Aliakbarian, F. Sadat Saleh, M. Salzmann, B. Fernando, L. Petersson, and L. Andersson. Encouraging lstms to anticipate actions very early. In *The IEEE International Conference on Computer Vision (ICCV)*, Oct 2017. 8
- [26] J. Walker, K. Marino, A. Gupta, and M. Hebert. The pose knows: Video forecasting by generating pose futures. In *Computer Vision (ICCV), 2017 IEEE International Conference on*, pages 3352–3361. IEEE, 2017. 1, 2, 5, 6, 7, 8
- [27] R. J. Williams and D. Zipser. A learning algorithm for continually running fully recurrent neural networks. *Neural computation*, 1(2):270–280, 1989. 12
- [28] X. Yan, A. Rastogi, R. Villegas, K. Sunkavalli, E. Shechtman, S. Hadap, E. Yumer, and H. Lee. Mt-vae: Learning motion transformations to generate multimodal human dynamics. In *European Conference on Computer Vision*, pages 276–293. Springer, 2018. 1, 2, 5, 6, 7, 8
- [29] D. Yang, S. Hong, Y. Jang, T. Zhao, and H. Lee. Diversity-sensitive conditional generative adversarial networks. In *International Conference on Learning Representations*, 2019. 6
- [30] Y. Yuan and K. Kitani. Diverse trajectory forecasting with determinantal point processes. *arXiv preprint arXiv:1907.04967*, 2019. 6

- [31] W. Zhang, M. Zhu, and K. G. Derpanis. From actemes to action: A strongly-supervised representation for detailed action understanding. In *Proceedings of the IEEE International Conference on Computer Vision*, pages 2248–2255, 2013. 6

A. Derivation of LCP-VAE’s KL Divergence Loss

In our approach, the model encourages the posterior of LCP-VAE to be close to the one of CS-VAE. In general, the KL divergence between two distributions P_1 and P_2 is defined as

$$\mathcal{D}_{KL}(P_1||P_2) = \mathbb{E}_{P_1} \left[\log \frac{P_1}{P_2} \right]. \quad (11)$$

Let us now consider the case where the distributions are multivariate Gaussians $\mathcal{N}(\mu, \Sigma)$ in \mathbb{R}^d , where $\Sigma = \text{diag}(\sigma^2)$, with σ and μ are d -dimensional vectors predicted by the encoder network of the VAE. The density function of such a distribution is

$$p(x) = \frac{1}{(2\pi)^{\frac{d}{2}} \det(\Sigma)^{\frac{1}{2}}} \exp \left(-\frac{1}{2} (x - \mu)^T \Sigma^{-1} (x - \mu) \right). \quad (12)$$

Thus, the KL divergence between two multivariate Gaussians is computed as

$$\begin{aligned} \mathcal{D}_{KL}(P_1||P_2) &= \frac{1}{2} \mathbb{E}_{P_1} \left[-\log \det \Sigma_1 - (x - \mu_1)^T \Sigma_1^{-1} (x - \mu_1) \right. \\ &\quad \left. + \log \det \Sigma_2 + (x - \mu_2)^T \Sigma_2^{-1} (x - \mu_2) \right] \\ &= \frac{1}{2} \left[\log \frac{|\Sigma_2|}{|\Sigma_1|} - d + \text{tr}\{\Sigma_2^{-1} \Sigma_1\} \right. \\ &\quad \left. + (\mu_2 - \mu_1)^T \Sigma_2^{-1} (\mu_2 - \mu_1) \right]. \end{aligned} \quad (13)$$

where $\text{tr}\{\cdot\}$ denotes the trace operator. In Eq. 13, the covariance matrix Σ_1 and mean μ_1 correspond to distribution P_1 and the covariance matrix Σ_2 and mean μ_2 correspond to distribution P_2 .

Given this result, we can then compute the KL divergence of the LCP-VAE and the posterior distribution with mean $\mu + \sigma \odot \mu_c$ and covariance matrix $\text{diag}((\sigma \odot \sigma_c)^2)$. Let $\Sigma = \text{diag}(\sigma^2)$, $\Sigma_c = \text{diag}(\sigma_c^2)$, and d be the dimensionality of the latent space. The loss in Eq. 6 of the main paper can then be written as

$$\begin{aligned} \mathcal{L}_{prior}^{\text{LCP-VAE}} &= -\frac{1}{2} \left[\log \frac{|\Sigma_c|}{|\Sigma_c||\Sigma|} - d + \text{tr}\{\Sigma_c^{-1} \Sigma_c \Sigma\} + \right. \\ &\quad \left. (\mu_c - (\mu + \Sigma \mu_c))^T \Sigma_c^{-1} (\mu_c - (\mu + \Sigma \mu_c)) \right]. \end{aligned} \quad (14)$$

Table 6. Quantitative evaluation on the Penn Action dataset. Note that a diversity of 1.21 is reasonably high for normalized 2D joint positions, i.e., values between 0 and 1, normalized with the width and the height of the image.

Method	Test MSE (KL) (Reconstructed)	Diversity (Sampled)	Quality (Sampled)	Context (Sampled)
LCP-VAE	0.034 (6.07)	1.21	0.46	0.70
AR Counterpart	0.048 (N/A)	0.00	0.46	0.51

Since $\Sigma_c^{-1} \Sigma_c = I$, $|\Sigma_c|$ will be cancelled out in the log term, which yields

$$\begin{aligned} \mathcal{L}_{prior}^{\text{LCP-VAE}} &= -\frac{1}{2} \left[\log \frac{1}{|\Sigma|} - d + \text{tr}\{\Sigma\} \right. \\ &\quad \left. + (\mu_c - (\mu + \Sigma \mu_c))^T \Sigma_c^{-1} (\mu_c - (\mu + \Sigma \mu_c)) \right]. \end{aligned} \quad (15)$$

B. Experimental Results on the Penn Action Dataset

As a complementary experiment, we evaluate our approach on the Penn Action dataset, which contains 2326 sequences of 15 different actions, where for each person, 13 joints are annotated in 2D space. Most sequences have less than 50 frames and the task is to generate the next 35 frames given the first 15. Results are provided in Table 6. Note that the upper bound for the Context metric is 0.74, i.e., the classification performance given the Penn Action ground-truth motions.

C. Additional Qualitative Results

Here, we provide qualitative results on diverse human motion prediction on the Human3.6M dataset. As can be seen in Figures 5 to 10, the motions generated by our approach are diverse and natural, and mostly within the context of the observed motion.

D. Stochastic Human Motion Prediction Architecture

Our motion prediction model follows the architecture depicted in Fig. 2 of the main paper. Below, we describe the architecture of each component in our model. Note that human poses, consisting of 32 joints in case of the Human3.6M dataset, are represented in 4D quaternion space. Thus, each pose at each time-step is represented with a vector of size 1×128 . All the tensor sizes described below ignore the mini-batch dimension for simplicity.

The **observed motion encoder**, or CS-VAE motion encoder, is a single layer GRU [7] network with 1024 hidden units. If the observation sequence has length T_{obs} , the observed motion encoder maps $T_{obs} \times 128$ into a single hidden representation of size 1×1024 , i.e., the hidden state of the



Figure 5. Qualitative evaluation of the diversity in human motion. The first row illustrates the ground-truth motion. The first six poses of each row depict the observation (the condition) and the rest are sampled from our model. Each row is a randomly sampled motion (not cherry picked). As can be seen, all sampled motions are natural, with a smooth transition from the observed to the generated ones. The diversity increases as we increase the sequence length.



Figure 6. Additional qualitative evaluation of the diversity in human motion.

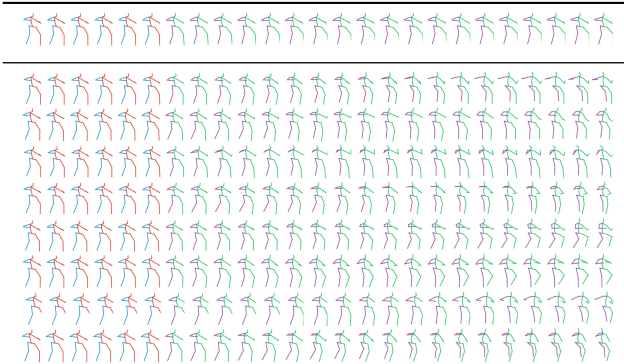


Figure 7. Additional qualitative evaluation of the diversity in human motion.

last time-step. This hidden state, h_t , acts as the condition to the LCP-VAE encoder and the direct input to the CS-VAE encoder.

CS-VAE, similarly to any variational autoencoder, has

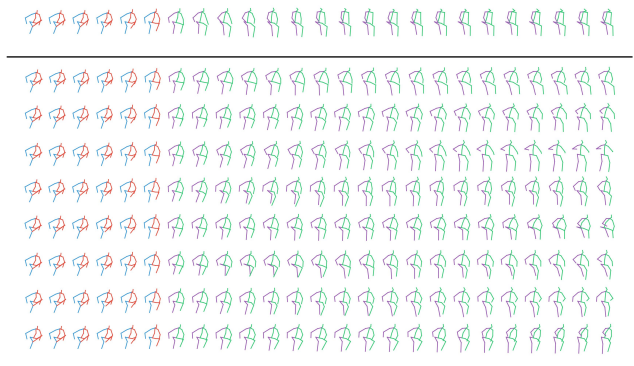


Figure 8. Additional qualitative evaluation of the diversity in human motion.



Figure 9. Additional qualitative evaluation of the diversity in human motion.



Figure 10. Additional qualitative evaluation of the diversity in human motion.

an encoder and a decoder. The CS-VAE encoder is a fully-connected network with ReLU non-linearities, mapping the hidden state of the motion encoder, i.e., h_t , to an embedding of size 1×512 . Then, to generate the mean and standard deviation vectors, we use two fully connected branches. They map the embedding of size 1×512 to a mean vector of size 1×128 and a standard deviation vector of size 1×128 , where 128 is the length of the latent variable. Note that we apply a ReLU non-linearity to the vector of standard deviation.

tions to ensure that it is non-negative. We then use the reparameterization trick [14] to sample a latent variable of size 1×128 . The CS-VAE decoder consists of multiple fully-connected layers, mapping the latent variable to a variable of size 1×1024 , acting as the initial hidden state of the observed motion decoder. Note that we apply a Tanh non-linearity to the generated hidden state to mimic the properties of a GRU hidden state.

The **observed motion decoder**, or CS-VAE motion decoder, is similar to its motion encoder, except for the fact that it reconstructs the motion autoregressively. Additionally, it is initialized with the reconstructed hidden state, i.e., the output of the CS-VAE decoder. The output of each GRU cell at each time-step is then fed to a fully-connected layer, mapping the GRU output to a vector of size 1×128 , which represents a human pose with 32 joints in 4D quaternion space. To decode the motions, we use a teacher forcing technique [27] during training. At each time-step, the network chooses with probability P_{tf} whether to use its own output at the previous time-step or the ground-truth pose as input. We initialize $P_{tf} = 1$, and decrease it linearly at each training epoch such that, after a certain number of epochs, the model becomes completely autoregressive, i.e., uses only its own output as input to the next time-step. Note that, at test time, the motions are generated completely autoregressively, i.e., with $P_{tf} = 0$.

Note that the future motion encoder and decoder have exactly the same architectures as the observed motion ones. The only difference is their input, where the future motion is represented by poses from T_{obs} to T_{end} in a sequence. In the following, we describe the architecture of LCP-VAE for motion prediction.

LCP-VAE is a conditional variational encoder. Its encoder’s input is a representation of future motion, i.e., the last hidden state of the future motion encoder, h_T , conditioned on h_t . The conditioning is done by concatenation, thus the input to the encoder is a representation of size 1×2048 . The LCP-VAE encoder, similarly to the CS-VAE encoder, maps its input representation to an embedding of size 1×512 . Then, to generate the mean and standard deviation vectors, we use two fully connected branches, mapping the embedding of size 1×512 to a mean vector of size 1×128 and a standard deviation vector of size 1×128 , where 128 is the length of the latent variable. Note that we apply a ReLU non-linearity to the vector of standard deviations to ensure that it is non-negative. To sample the latent variable, we use our extended reparameterization trick, explained in the main paper. This unifies the conditioning and sampling of the latent variable. Then, similarly to CS-VAE, the latent variable is fed to the LCP-VAE decoder, which is a fully connected network that maps the latent representation of size 1×128 to a reconstructed hidden state of size 1×1024 for future motion prediction. Note that we apply

a Tanh non-linearity to the generated hidden state to mimic the properties of a GRU hidden state.